IAHR AIRH

26th IAHR International Symposium on Ice
Montréal, Canada – 19-23 June 2022

Investigating the dominant force distributions in ice-induced vibrations using multivariate analysis

Grant Peel, Ersegun Deniz Gedikli
Department of Ocean and Resources Engineering, University of Hawaii at Manoa, Honolulu, HI 96822
gjpeel@hawaii.edu, egedikli@hawaii.edu

When subjected to ice-induced vibrations, the dynamics of offshore structures in the Arctic and Sub-Arctic areas are known to exhibit complex non-linear behavior. Parameters such as ice drift velocity, ice drift direction, ice thickness, ice and/or air temperature, for example, change over time throughout the operation and may cause the structure to oscillate with large amplitude motions. The resulting motions may be regular or irregular depending on the nonlinear nature of the force distribution on the structure, and may cause fatigue-related damage to the structure if disregarded in design or not adequately monitored. Many models that predict ice-induced vibrations do not discuss this fact, hence use simple force models. In this paper, we apply multivariate analysis techniques to examine the measured force distributions on the Norströmsgrund lighthouse. As a result, we 1) identify the active force panels during ice-structure interactions, 2) demonstrate the extremely variable ice drift directions in early and late seasons, 3) show the energy contribution of each force panels and relate them to ice drift directions, and 4) reveal the dominant force modes using proper-orthogonal decomposition. The potential of a data-driven force model that captures the nonlinear nature of the force distribution in ice-induced vibrations is discussed.

1. Introduction

The ice infested Arctic and Sub-Arctic regions are a harsh environment for ships and offshore structures to be located and operated in. Being exposed to ice, these structures can sustain serious damage during the ice-structure interactions. Ice Induced Vibrations (IIVs) can result in significant

structural movements which in turn can greatly reduce the fatigue life of the structure. During these interactions the structures may experience resonance which occurs when the vibrations are oscillating at a frequency near the structure's natural frequency. This results large observed amplitudes. These large amplitude vibrations are referred to as frequency lock-in (henceforth known as FLI) events (Nord et al., 2018).

The LOLEIF (Low Level Ice Forces) and STRICE (Measurements on Structures in Ice) datasets are among the most complete datasets on ice-structure interactions and have been thoroughly analyzed as such. These datasets are focused on the Norströmsgrund Lighthouse located at the head of the Gulf of Bothnia (N 65º 6.6' E 22º 19.3') during the winters of 2000 to 2003. During this period, nine force panels were installed at 14.5 meters above the seabed on the Mean Water Line (MWL), as shown in Figure 1. The force panels covered 162º of the outer perimeter and were only placed on the North to Southeast section of the lighthouse (Frederking, 2005). This was because the prevailing ice direction was thought to be from the land fast ice decoupling from the shore and drifting with the prevailing winter winds from the Northeast (Gedikli et al., 2020).

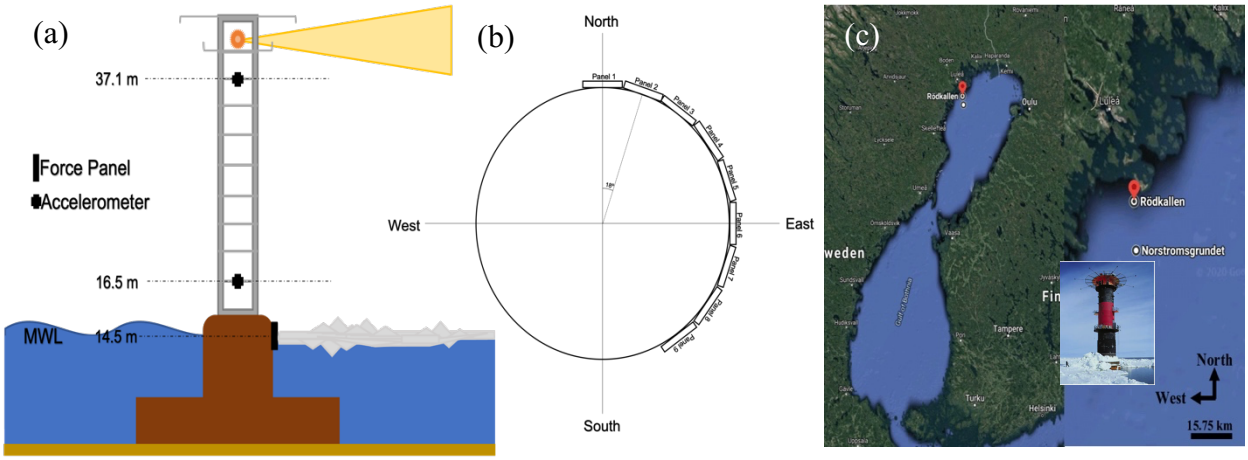

Figure 1. Layout of the Norströmsgrund Lighthouse. (a) profile view of the lighthouse showing the vertical layout of the accelerometers and force panels relative to the seabed and MWL. (b) top view of the lighthouse showing the load panel orientation (using the altered numbering system) with the top oriented North. (c) location of the lighthouse relative to the closest weather station at Rødkallen (on right) and the Gulf of Bothnia (on left).

In their paper, Nord et al. (2018) identified 61 FLI events on the Norströmsgrund Lighthouse during the winters between 2001 and 2003. These FLI events were identified by finding all instances that the upper accelerometer on the lighthouse had an magnitude greater than $0.07\ g$ ($0.686\ m/s^2$) and a dominant frequency between 2.0 and $2.7\ Hz$ (which was the designated range for resonant vibrations for this structure/ice system).

In this study, we revisit these events and employ a multivariate analysis technique known as proper-orthogonal decomposition (POD, (Feeny and Kappagantu, 1998), (Gedikli and Dahl, 2017)) to identify the active force panels, the amount of energy held by each force panel, and how the force load on the structure is distributed during these events. We apply this method to both dynamic and the total force data, and compare the results.

2. Methods

First, we recreate the data matrix, which includes 61 of the IIV events identified by Nord et al. (2018). The start and end times listed in the Table 2 of Nord et al. (2018) were used as indices to ensure the signals used in this paper were the same compared in the past literature. The force measurements from each panel were then loaded and cut based on the identified indices, and the panels were reordered to be more intuitive for the viewers (with the panel 1 oriented North and each subsequent panel ordered 2 through 9). The force signal in each panel was then split into static and dynamic components by running the force data through a low pass filter for the static component and a high pass filter for the dynamic component. POD was then performed on both the dynamic component of the force as well as the total force.

POD is a matrix decomposition technique and can be expressed as an optimization problem. POD looks for an orthogonal coordinate system with a small number of coordinates that can maximize the expression of variance in the data. According to Feeny and Kappagantu (1998); Ilbeigi and Chelidze (2017); Gedikli et al. (2017); Gedikli and Dahl (2017); Peel and Gedikli (2022), when the field $\{u(x,t)\}$ is sampled such that $X_{ij} = u(x_j, t_i)$, where $X \in \Re^{m \times n}$, then POD can be solved by singular value decomposition $X = P\sigma V^T$, where σ values represents the POVs, $P\sigma$ represents the time coordinates (POCs) and V contains the corresponding mode shapes (POMs). In POD, proper orthogonal modes (POMs) represent spatial modes, proper orthogonal coordinates (POCs) represent temporal modes, and proper orthogonal values (POVs) represent the proxy of kinematic energy of each mode (or subspace dimension). Mode shapes (or POMs) represent the spatial distribution of force in our case (i.e., half sinusoidal loading on the structure). But first mode is not necessarily a half-sinusoid; it is the shape corresponding to the highest singular value in the system, as described by the system's energy (see Eq. 1).

The cumulative energy in the system can be calculated by adding all the modes up to the i^{th} mode and dividing by the total response

$$E_i = \frac{\sum_j^i \sigma_j}{\sum_j^p \sigma_j} \times 100\% \quad (1)$$

where σ_j represents the value of the j^{th} POV and p indicates the number of the total modes identified using POD. In this study, the number of modes required to represent 90 percent of the force signal was estimated cumulatively using Eq. 1. Minimum number of modes required to exceed the 90 percent criterion is referred to as ii which was used to reconstruct the signal. Using ii, each force panel's contribution to the total energy in the system, referred to as relative energy contribution is calculated by multiplying the POVs with the POMs. Using the relative energy contribution, panels that contributed greater than or equal to 5% of the total energy in the system were identified.

Figure 2 is an example POD reconstruction for Event 53 in Nord et al. (2018), demonstrating that the first three modes of the Event 53's dynamic component account for 80 percent of the total signal (all panels included). Furthermore, when individual panels are evaluated, it has an RMSE of $4.936\ kN$ for panel 4 (see Fig.1 for panel descriptions).

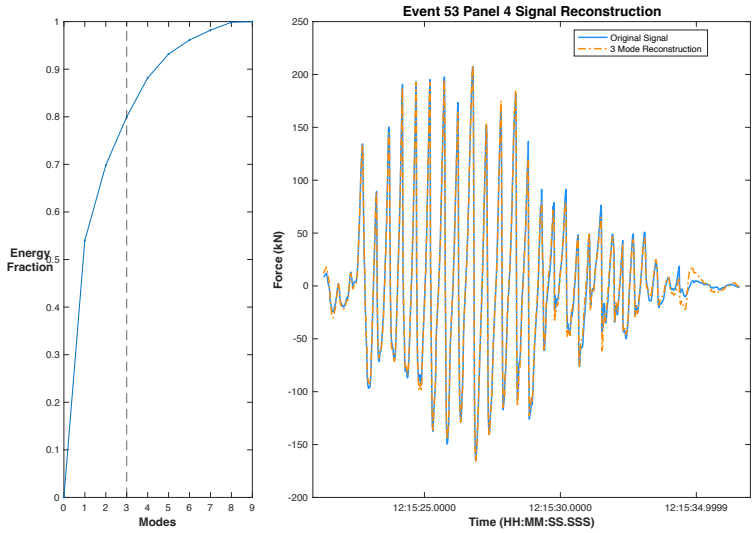

Figure 2. Comparison of the reconstructed signal versus the original signal force panel 4. The first 3 modes of event 53's dynamic component represent 80% of the entire signal (all panels included) but the RMSE for panel 4 is 4.936 kN.

The weighted *circular mean* ($\overline{\Psi_\iota}$) was calculated for all panels and all panels that exceeded the threshold based on panel orientation using the following formula where the directions are first transformed to unit vectors in the two-dimensional plane, and then vector averaged.

$$\Psi_i = \begin{pmatrix} \cos\alpha_i \\ \sin\alpha_i \end{pmatrix} \quad \rightarrow \quad \overline{\Psi_\iota} = \frac{1}{N}\sum_i \Psi_i \tag{2}$$

where N is the total number of panels, α is the angle at the center of the panel relative to the structural orientation in Fig.1b, Ψ_i represents the transformed vectors and $\overline{\Psi_\iota}$ represents the mean resultant vector. For more information regarding the circular means, readers of this work are encouraged to read (Berens, 2009; Gedikli et al., 2020). The circular variance (CV) of a set of dihedral angles is calculated using Eq. 3 where n is the number of members in the ensemble. In other words the CV shows how tightly or loosely a residue's torsion angles cluster across all models (Berens, 2009). Equation 4 represents the root-mean-squared error angle (θ_{RMSE}) of the metric (i.e. wind direction, force direction etc.) relative to the ice direction reported in the logbook. Equation 5 represents the mean absolute value of errors of the relative angle θ.

$$CV = 1 - \frac{1}{n}\sqrt{\left(\sum_{i=1}^{n} cos\theta_i\right)^2 + \left(\sum_{i=1}^{n} sin\theta_i\right)^2} \tag{3}$$

$$\theta_{RMSE} = \sqrt{\frac{\sum_{i=1}^{n}\theta_i^2}{n}} \tag{4}$$

$$MAE = \frac{\sum_{i=1}^{n} |\theta_i|}{n} \quad (5)$$

3. Results and Discussion

The calculated total forces from the force measurements have both a dynamic part and a slowly varying static part. A high pass filter is applied to eliminate the static part, so that the remaining dynamic part can be used to identify the dominant force modes. It is also known that each event does not necessarily have the same sampling size (Tu et al., 2019). However, because we are only interested in the dominant force distribution in a single event, each event is not resampled to obtain a uniform sampling size for all events. However, if we want to compare the events and use the resulting distribution for general force modeling, we must have the same sampling size.

Figures 3,4,5 and 6 represent four example IIV events (Events 6, 18, 42 and 53) where POD is applied to the dynamic force components. Left image in these figures represent the top view of the structure illustrating the active force panels and the directions of wind, ice, and POD identified dominant force directions. Center images represent relative energy in each mode (top image), POMs (center image), and scaled POMs (or relative energy in each force panels). Right image in Figure 4 illustrate the distribution of total forces on the panels.

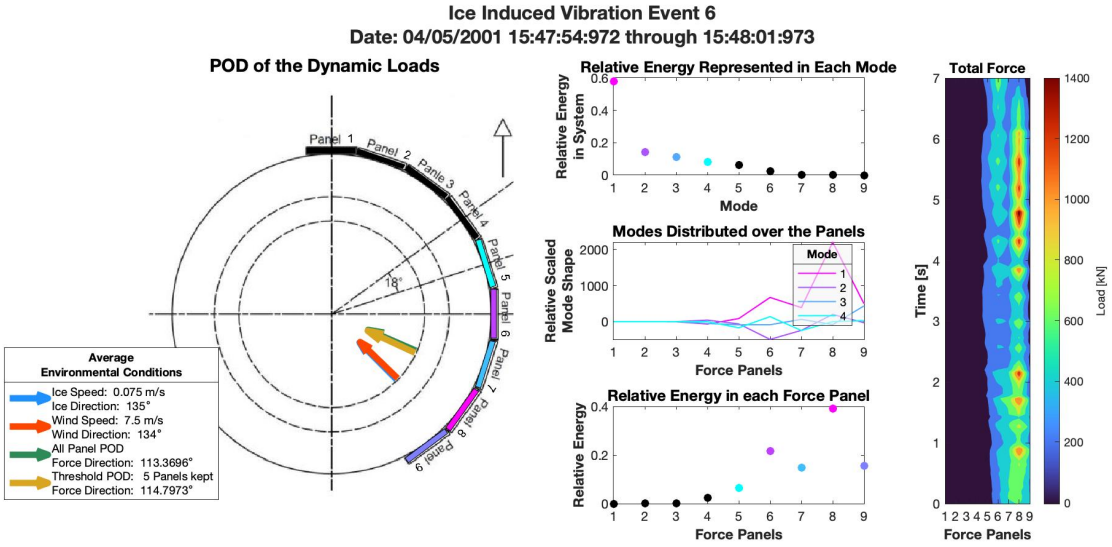

Figure 3. POD of IIV Event 6 that occurred on April 5, 2001. Left image: Top view of the structure with active force panels and environmental conditions. Center image: Top image represents relative energy in each mode, center image represents POMs and bottom image represents the scaled POMs. Right image: Total force distribution.

In Event 6, the ice and wind directions are at 135º and the identified dominant force direction is at 115º, implying that more energy is impacted at 115º on the force panel 7 than on panels 8 or 9. When the contribution of each force panel is analyzed, it is interesting to see that there is more relative energy in force panel 6 than in either 7 or 9, but panel 8 has the dominant energy (see center bottom image in Fig.3). This implies that force distribution is not homogeneous along the structure's perimeter. More importantly, the most prevalent mode has a half-sinusoid form with a peak at panel 8 and corresponds to 60% of the energy in the system (center-top image in Fig.3),

which can be also seen in the total force distribution graphic (far right image in Fig.3). This quantification is essential for future force modeling. After analyzing the event footage, the ice appears to be consistent level ice that is affecting across panels 5 through 9 (the panels registering above the threshold). The event featured more extreme environmental circumstances than the average reported FLI event, with an ice thickness of 0.9 $meters$ and a velocity of 0.075 m/s.

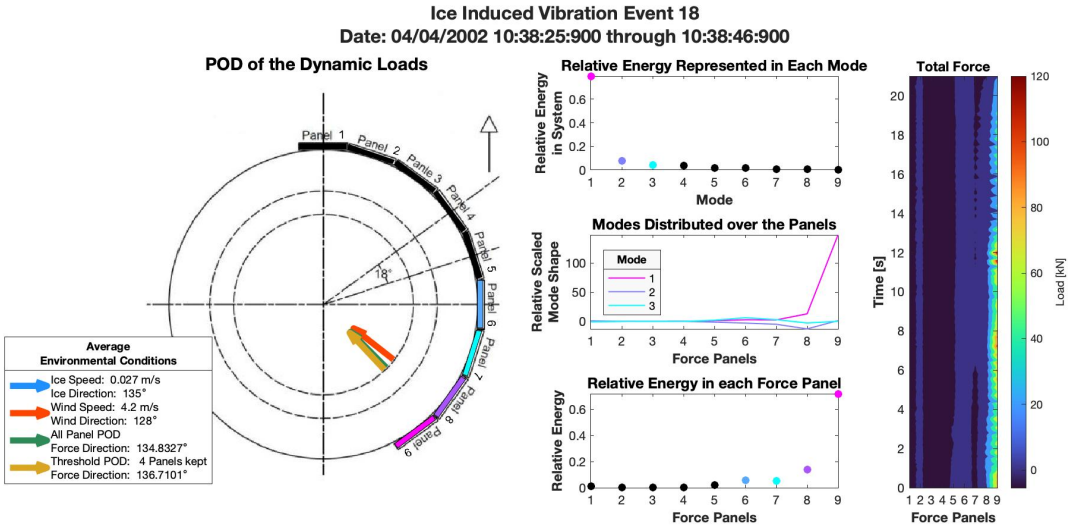

Figure 4. POD of IIV Event 18 that occurred on April 4, 2002. Left image: Top view of the structure with active force panels and environmental conditions. Center image: Top image represents relative energy in each mode, center image represents POMs and bottom image represents the scaled POMs. Right image: Total force distribution.

Figure 4 illustrates the POD data for event 18 from April 4th, 2002, one of the most precisely measured events. The force was relatively moderate in comparison to the other events, with the ice thickness and velocity being lower than the average FLI event (0.4 m vs 0.82 m and 0.027 m/s vs 0.043 m/s). Despite the fact that the stated ice drift direction is the same as in event 6 (between panels 8 and 9), force panel 9 was the dominating force panel during this event. With panel 8 and 9 experiencing almost 80% of the energy, the weighted average was not as influenced by the sampling bias caused by a lack of panel coverage as it was in Event 6. Unfortunately, a dominant force mode is not observed in this event because the ice-structure interaction surface is not completely covered by the force panels (i.e., there is also ice coming from the south but no force measurement).

Figure 5 depicts the POD results for Event 42 from March 25th, 2003, one of the two IIV observed event days in which more than half of the FLI events occurred throughout the study period. The ice drift direction is south (180º), which is slightly off of the panels, but with all of the energy concentrated on the edge panel (9) it shows how the force does not spread far from the incident angle. As a result, similar to Event 18, no dominant force distribution is seen. Because of the structure's insufficient panel coverage, POD identified force direction is also inaccurate in this event.

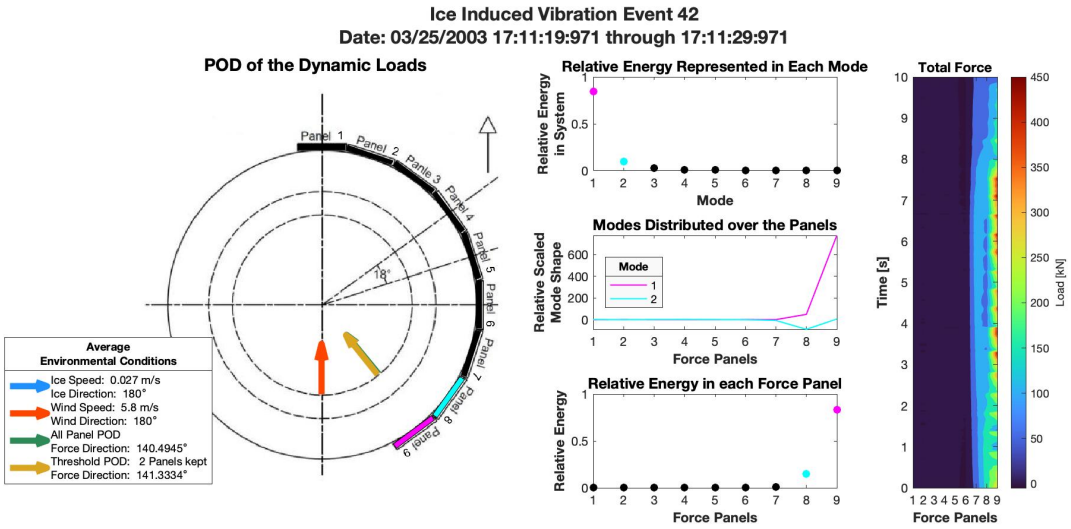

Figure 5. POD of IIV Event 42 that occurred on March 25, 2003. Left image: Top view of the structure with active force panels and environmental conditions. Center image: Top image represents relative energy in each mode, center image represents POMs and bottom image represents the scaled POMs. Right image: Total force distribution.

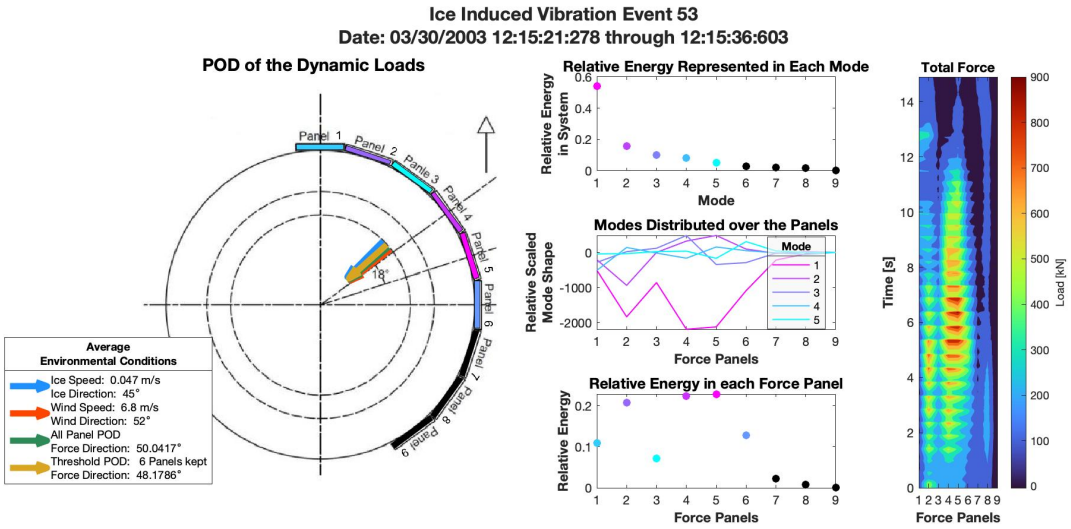

Figure 6. POD of IIV Event 53 that occurred on March 30, 2003. Left image: Top view of the structure with active force panels and environmental conditions. Center image: Top image represents relative energy in each mode, center image represents POMs and bottom image represents the scaled POMs. Right image: Total force distribution.

Figure 6 shows the POD data for Event 53 from March 30th, 2003, one of the extreme IIV events in which the force panels were continually impacted with ice for an extended period of time. The ice drift direction was 45º, which resulted in better balanced forces, with 5 panels contributing more than 10% energy and 3 panels contributing more than 20%. This event illustrates how modes are not restricted to a single force panel, as evidenced by the relative mode shape. There is an interesting decrease in energy in force panel 3 when compared to the force panels around it, which

could indicate a weaker portion of ice (ridge ice collapsing on the structure). The most prevalent mode, like Event 6, has a half-sinusoid shape with a peak at panels 4 and 5, and corresponds to nearly 60% of the total energy in the system.

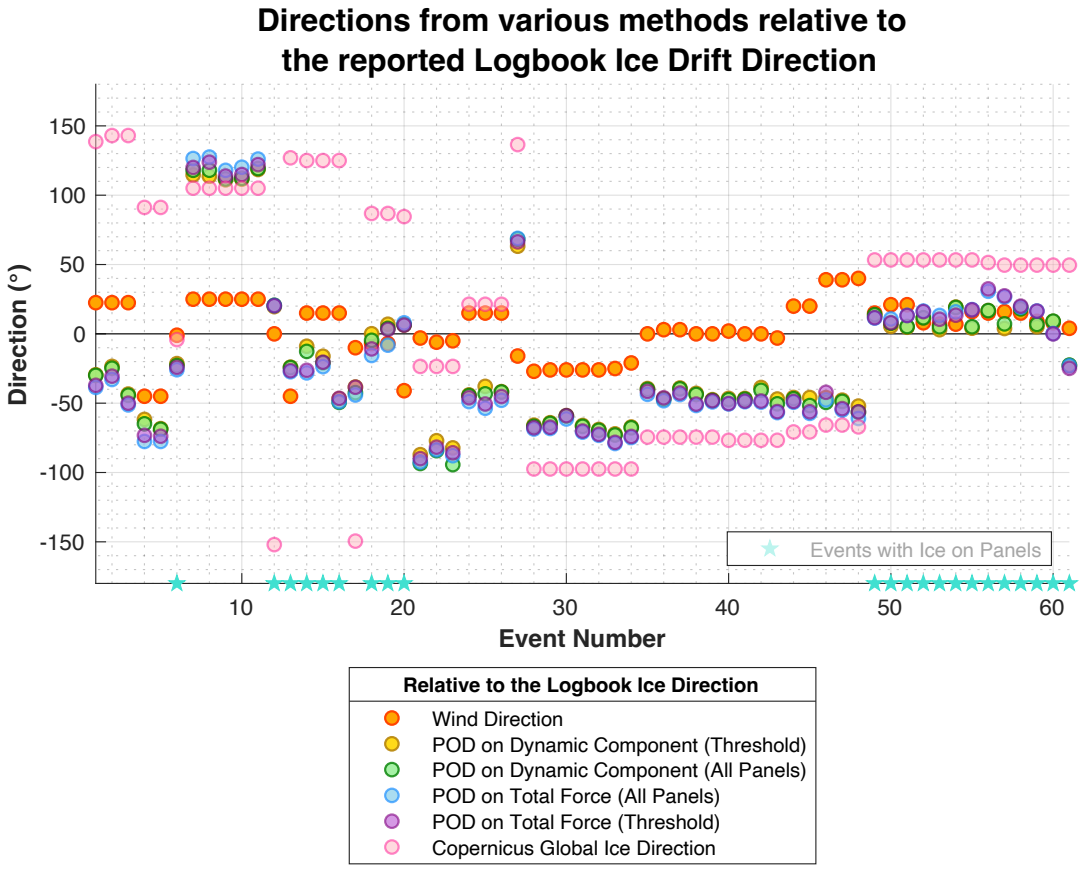

Figure 7. Force directions compared to ice drift directions for each logbook occurrence. The wind directions are from the logbook and the Global ice directions are from the Copernicus sampled at a 1/12º resolution (Turner et al., 2020). Blue stars show which FLI events occurred with the ice impacting inside the panel range

Figure 7 compares the wind, POD, and Copernicus global ice directions to the logbook ice drift directions. The error metrics estimated for 1) events with ice on panels and 2) all 61 occurrences that resulted in IIVs are shown in Table 1. As illustrated in Figure 7 and Table 1, the POD prediction of ice drift direction works reasonably well when the ice collides with the force panels (i.e. when there is ice on the panels, the calculated errors are much smaller than the error calculated using all of the events). Other significant findings include: 1) for the occurrences with ice on panels, all of the metocean angle data are close to one another; and 2) the wind direction is close to the observed ice drift direction, confirming that ice is driven by the wind. It should be noted that these results are based on logbook data collected during each IIV event; nevertheless, Gedikli et al. (2020) demonstrated that ice drift and wind directions do not always point in the same direction on the same day that an IIV is recorded. The relative energy threshold of the POD of the dynamic component, which had less variability than even the wind direction, was found to be the best approach for identifying the dominant ice drift direction.

It is critical to identify the dominant force distribution for accurate force modeling. The POD data will then be used in conjunction with equation free modeling, as described by Brunton et al. (2016), to generate several empirical equations to recreate the force distribution and thus force modeling. It is hypothesized that these equations will be nonlinear and involve many parameters that will correlate with the most important environmental data, such as ice direction, ice concentration, and ice thickness.

	Circular Variance (CV)		Root Mean Squared Error (RMSE)		Mean Absolute Value of Errors (MAE)	
	All Events	Ice on Panels	All Events	Ice on Panels	All Events	Ice on Panels
Wind Direction	0.0629	0.0421	20.90º	17.67º	16.75º	14.00º
POD on Dynamic Component (Threshold)	0.2848	0.0410	53.28º	16.63º	43.46º	13.09º
POD on Dynamic Component (All Panels)	0.2995	0.0457	55.18º	17.56º	45.32º	14.29º
POD on Total Force (All Panels)	0.3300	0.0686	59.15º	21.53º	50.05º	19.13º
POD on Total Force (Threshold)	0.3192	0.0634	57.16º	20.73º	48.16º	18.00º
Copernicus Global Ice Direction	0.8280	0.2264	86.85º	80.67º	79.40º	72.22º

Table 1. Error metrics values for wind direction, Copernicus global ice direction, and POD-based force direction using circular variance (CV), RMSE, and MAE

5. Conclusion

Panel force data from the 61 FLI events identified in Nord et al. (2018) were decomposed using POD, and the number of modes required to represent at least 90% of the signal was identified. The POVs and POMs were used to calculate the relative energy contribution of each panel, and then a 5% threshold was applied to determine which panels were significant during the event.

- POD can be used to determine the dominant ice drift directions. Although the use of POD is currently limited to the 22 cases where ice interacts with the panels. It is possible to identify the dominant POMs as long as the force is measured.
- Even though the ice is hitting the structure on the panels, POD shows that force is not always uniformly distributed along the perimeter of the structure. These occurrences must be investigated further in light of the ice type and environmental conditions.
- The sum of the first three dominant modes almost always accounts for more than 80% of the kinetic energy in the system, implying that the first three mode shapes associated with these modes may be associated with forces in three different directions (xyz), as discussed in Gedikli et al (2019). This needs to be further investigated.
- The ice directions reported in the logbooks, as well as the wind and force directions, are comparable and agree well.

Acknowledgements

Grant Peel and E. Deniz Gedikli acknowledge support on this work from the National Science Foundation (PM: Mamadou Diallo) under award no. 2127095.

References

Berens, P., 2009. CircStat: A MATLAB Toolbox for Circular Statistics. Journal of Statistical Software 31, 1–21. https://doi.org/10.18637/jss.v031.i10

Brunton, S.L., Proctor, J.L., Kutz, J.N., 2016. Discovering governing equations from data by sparse identification of nonlinear dynamical systems. Proceedings of the National Academy of Sciences 113, 3932–3937. https://doi.org/10.1073/pnas.1517384113

Feeny, B.F., Kappagantu, R., 1998. ON THE PHYSICAL INTERPRETATION OF PROPER ORTHOGONAL MODES IN VIBRATIONS. Journal of Sound and Vibration 211, 607–616. https://doi.org/10.1006/jsvi.1997.1386

Frederking, R., 2005. Tiltmeter Application at Norströmsgrund Lighthouse - Strice Project, in: Proceedings of the International Conference on Port and Ocean Engineering Under Arctic Conditions. Presented at the 18th International Conference on Port and Ocean Engineering under Arctic Conditions (POAC'05).

Gedikli, E.D., Bjerkås, M., Høyland, K.V., Hornnes, V., Turner, J.D., 2020. On the ice and wind conditions in the northern part of the Gulf of Bothnia leading ice-induced vibrations, 188-198. The International Association for Hydro-Environment Engineering and Research (IAHR).

Gedikli, E.D., Dahl, J.M., 2017. Mode excitation hysteresis of a flexible cylinder undergoing vortex-induced vibrations. Journal of Fluids and Structures 69, 308–322. https://doi.org/10.1016/j.jfluidstructs.2017.01.006

Gedikli, E.D., Dahl, J.M., Chelidze, D., 2017. Multivariate Analysis Of Vortex-Induced Vibrations In A Tensioned Cylinder Reveal Nonlinear Modal Interactions. Procedia Engineering, X International Conference on Structural Dynamics, EURODYN 2017 199, 546–551. https://doi.org/10.1016/j.proeng.2017.09.159

Gedikli, E.D., Nord, T.S., Hendrikse, H., Ziemer, G., 2019. On pressure modes in ice-induced vibrations using multivariate analysis. Cold Regions Science and Technology 160, 150–162. https://doi.org/10.1016/j.coldregions.2019.02.003

Ilbeigi, S., Chelidze, D., 2017. Persistent model order reduction for complex dynamical systems using smooth orthogonal decomposition. Mechanical Systems and Signal Processing 96, 125–138. https://doi.org/10.1016/j.ymssp.2017.04.005

Nord, T.S., Samardžija, I., Hendrikse, H., Bjerkås, M., Høyland, K.V., Li, H., 2018. Ice-induced vibrations of the Norströmsgrund lighthouse. Cold Regions Science and Technology 155, 237–251. https://doi.org/10.1016/j.coldregions.2018.08.005

Peel, G., Francis, O., Hendrikse, H., Gedikli, E.D., 2022. Navigating the New Arctic through investigating ice-structure interactions, in: Ocean Sciences Meeting. Presented at the Ocean Sciences Meeting, Hawaii.

Tu, Y., Nord, T.S., Høyland, K.V., Petersen, Ø.W., 2019. Statistical analysis of ice-induced loads on the norstromsgrund lighthouse. 2019-June.

Turner, J.D., Høyland, K.V., Hornnes, V., Gedikli, E.D., 2020. Comparison of in-situ measurements from the Norströmsgrund lighthouse to Copernicus reanalysis products, 252-262. The International Association for Hydro-Environment Engineering and Research (IAHR).